Dennis Zelle*, Ernst Dalhoff and Anthony W. Gummer

Time-domain analysis of distortion-product otoacoustic emissions using a hydrodynamic cochlea model

Abstract: As a by-product of nonlinear amplification in the cochlea, the inner ear emits sound waves in response to two tones with different frequencies. These sound waves are measurable in the ear canal as distortion-product otoacoustic emissions (DPOAEs). DPOAEs putatively consist of two components emerging at different locations in the cochlea. Wave interference between the two components limits the accuracy of DPOAEs as a noninvasive measure of cochlear function. Using short stimulus pulses instead of continuous stimuli, the two DPOAE components can be separated in the time domain due to their different latencies. The present work utilizes a nonlinear hydrodynamic cochlea model to simulate short-pulse DPOAEs in the time domain. When adding irregularities to the mechanical parameters of the model, the simulated DPOAE signals show two distinguishable components and long-lasting beat tones, similar to band-pass filtered experimental data from normal-hearing human subjects. The model results suggest that the beat tones can occur solely due to interference of the coherent-reflection component with the fading nonlinear-distortion component.

Keywords: cochlear amplifier, distortion products, wave interference, otoacoustic emissions

https://doi.org/10.1515/cdbme-2017-0095

1 Introduction

Distortion-product otoacoustic emissions (DPOAEs) are sound waves measurable in the ear canal that emerge in response to two primary tones with frequencies f_1 and f_2 (typically f_2/f_1 = 1.2) due to nonlinear amplification of hydrodynamic oscillations in the cochlea [1, 2]. Hydrodynamic oscillations initiated by stapes motion propagate along the basilar membrane (BM), forming a pattern known as a traveling wave (TW) (Figure 1B). The location of the TW peak on the BM is a function of frequency, with high-frequency waves localized in the basal region near the stapes, and low-frequency waves traveling to the apical part near the helicotrema. Hence, each frequency has its own characteristic site on the BM, referred to as the tonotopic place [2].

Cochlear amplification increases the amplitude of the TW locally near the tonotopic place, therefore, enabling the high sensitivity, high frequency resolution, and wide dynamic range of the auditory system [2]. The most prominent DPOAE in humans occurs at the cubic difference frequency, $f_{DP} = 2f_1 - f_2$, and is supposed to consist of two components arising by different mechanisms at different locations on the BM [3]. The first component, the nonlinear-distortion component, emerges directly from the nonlinear interaction of the primary tones close to the f_2-tonotopic place, where the primary-tone traveling waves overlap maximally. The nonlinear-distortion component produces a third traveling wave propagating to the f_{DP}-tonotopic place, where it is partially reflected, putatively due to coherent reflection at mechanical irregularities of the cochlear partition, giving rise to the so-called coherent-reflection component.

Wave interference between the two components is a major limiting factor when using DPOAEs as an objective and noninvasive measure to evaluate the functional state of the cochlea [4]. Exploiting the different latencies of the components, stimulation with short pulses instead of conventional continuous primary tones enables the separation of the DPOAE components in the time domain [5], which significantly increases the accuracy of DPOAEs when used to estimate behavioral thresholds [4, 6]. However, there is evidence for additional components in the DPOAE recordings. The present work utilizes a one-dimensional

***Corresponding author: Dennis Zelle,** Section of Physiological Acoustics and Communication, Department of Otolaryngology, University of Tübingen, Elfriede-Aulhorn-Str. 5, 72076 Tübingen, Germany, e-mail: dennis.zelle@uni-tuebingen.de
Ernst Dalhoff, Anthony W. Gummer: Section of Physiological Acoustics and Communication, Department of Otolaryngology, University of Tübingen, Elfriede-Aulhorn-Str. 5, 72076 Tübingen, Germany, e-mail: ernst.dalhoff@uni-tuebingen.de, anthony.gummer@uni-tuebingen.de

implementation of a nonlinear hydrodynamic cochlea model to identify the origin of additional signals by comparing simulated distortion products with measured short-pulse DPOAE signals.

2 Materials and methods

2.1 Hydrodynamic cochlea model

The cochlea is modeled as two arrays of locally damped, harmonic oscillators representing the basilar-membrane (BM) and tectorial-membrane (TM) segments as function of longitudinal position x, normalized to BM length, i.e. x = 0 and x = 1 correspond to positions at the stapes and the helicotrema, respectively (Figure 1A). The BM elements incorporate the mass density $m(x)$ of the organ of Corti, the viscous damping $d(x)$ of the organ of Corti, and the stiffness $k(x)$ of the BM. $k(x)$ was specified so that the model reproduces the tonotopic map of the human cochlea [7]. Similarly, $\gamma_{TM}(x)$ and $\omega_{TM}(x)$ specify the damping ratio and the resonance frequency of a TM segment. $\omega_{TM}(x)$ was 0.5 octave below the resonance of the BM at x [8]. The cochlear fluids are assumed to be incompressible and irrotational. Thus, a pressure induced by the motion of the stapes at the oval window in scala vestibuli (SV) propagates instantaneously to the round window in scala tympani (ST) via the connection of SV and ST at the helicotrema. The resulting difference pressure drives the BM segments. Additionally, motion of a BM element at position $\tilde{x}$ (Figure 1A, red dot) acts as a local pressure source. The superposition of the pressure fields yields the hydrodynamic force

$$F_H(x,t) = G_s(x)\ddot{u}(t) + \int_{x=0}^{x=1} G(x,\tilde{x})\ddot{y}(\tilde{x},t)d\tilde{x} + F_{ca}(x,t) \quad (1)$$

acting on a cochlear partition at BM position x and time t. $G_s(x)\ddot{u}(t)$ and $G(x,\tilde{x})\ddot{y}(\tilde{x},t)$ are hydrodynamic force terms relating the pressure changes due to accelerations of the stapes, $\ddot{u}(t)$, and of the BM element, $\ddot{y}(\tilde{x},t)$, to the cochlear partition at x [9, 10]. Spatial integration over the fluid using isopotential surfaces (S_+, S_-) of the velocity potential yields the hydrodynamic coupling terms G_s (Figure 1A, gray dashed lines) and $G(x,\tilde{x})$ (red dash-dotted lines), respectively [10].

The force term $F_{ca}(x,t)$ replicates cochlear-amplifier force, which only acts in a local basal range close to the peak of the traveling wave (Figure 1B, black line). $F_{ca}(x,t)$ depends nonlinearly on stereocilia deflection, which is approximated by the radial displacement $z(x,t)$ of the TM [11, 12]. The blue line in Figure 1B depicts a snapshot of $\dot{z}(x,t)$. A three-state Boltzmann function, representing the dependence of the outer-hair-cell receptor current on $z(x,t)$ specifies the nonlinearity in the model [11]. Due to the different resonance frequencies of BM and TM, $F_{ca}(x,t)$ counteracts viscous damping only in a small basal region close to the tonotopic place, inducing local amplification of the traveling wave. In order to produce coherent reflection, roughness in form of Gaussian distributed variations in $k(x)$ and $F_{ca}(x,t)$ were incorporated in the model, with the standard deviation, R, given in percent of the parameters. Matrix formulation of the equation of motions enabled the computation of the solution directly in the time domain using Matlab (version 9.2, MathWorks, Natick, MA).

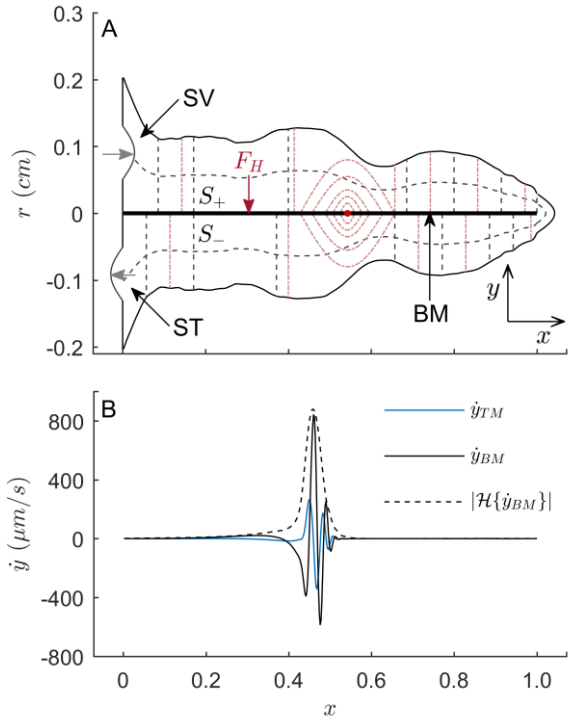

Figure 1: A: Scheme of the uncoiled cochlea. r: average radius of scala vestibuli (SV) and scala tympani (ST) as function of basilar-membrane (BM) position x. Gray inward arrow: displacement of oval window; gray outward arrow: displacement of round window. Red dot: local pressure source due to motion of a BM element at $\tilde{x}$. Spatial integration over the fluid using isopotential surfaces (S_+, S_-) of the velocity potential yields the hydrodynamic coupling terms G_s and $G(x,\tilde{x})$, which relate motion of the stapes (gray dashed lines) and the BM element (red dash-dotted lines) to the force F_H at x [10]. **B**: Traveling waves on BM (black solid line) and on tectorial membrane (blue) for an ear-canal stimulus with f = 2 kHz and L = 50 dB SPL. Black dashed line: envelope of BM traveling wave.

2.2 Experimental DPOAE data

Simulated distortion products were compared to short-pulse DPOAE signals recorded in normal-hearing subjects using an

ER-10C DPOAE probe-system (Etymotic Research, Elk Grove Village, IL) connected to a commercially available PC via a 16-bit analog output card, a 24-bit signal acquisition card, and LabVIEW (NI PCI 6733, NI PCI 4472, version 12.0, National Instruments, Austin, TX). The DPOAE was evoked using a short f_2 pulse in the presence of a longer f_1 pulse. Suitable phase shifts of the stimulus pulses in consecutive acquisition blocks enabled the cancelation of the stimulus pulses after ensemble averaging [13]. Details of the measurement setup and the short-pulse acquisition paradigm are specified elsewhere [6]. For comparison with simulated data, DPOAE components were extracted by fitting the zero-phase band-pass filtered signal with a mathematical model using a least-squares approach [5].

3 Results

3.1 Model performance

The model mimics general features of the human cochlea closely and exhibits large amplification and high tuning for low input levels, with a maximum gain of 52 dB at 4 kHz for L = 10 dB sound pressure level (SPL) in the ear canal. Amplification decreases towards apical and basal BM positions, with 30 dB at 0.5 kHz and 41 dB at 10 kHz. With decreasing frequency, the traveling waves increase in width, indicating less tuning in the apical region. For L = 10 dB SPL, Q_{10}, defined as the ratio of the frequency of the TW and its bandwidth 10 dB below the TW peak, decreases from 5.7 at 10 kHz to 1.9 at 0.5 kHz. Figure 2 depicts input-output functions of the BM velocity, $\dot{y}(x,t)$, for an active (solid line) and a passive (dashed line; $F_{ca}(x,t)$ = 0) cochlea for 2-kHz stimulation with increasing L. The active cochlea exhibits compressive amplification with a slope of 0.27 dB/dB at L = 50 dB SPL. Amplification and tuning decreases with increasing stimulus level, accompanied by a longitudinal shift of the TW peak towards a more basal position.

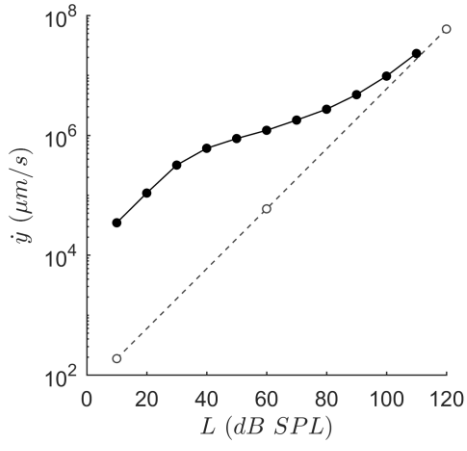

Figure 2: Input-output functions of the maximum BM velocity, $\dot{y}(x,t)$, as function of ear-canal pressure level L for f = 2 kHz. Dashed line: passive cochlea, i.e. F_{ca}= 0. Solid line: active cochlea with compressive amplification and 45-dB gain at L = 10 dB SPL.

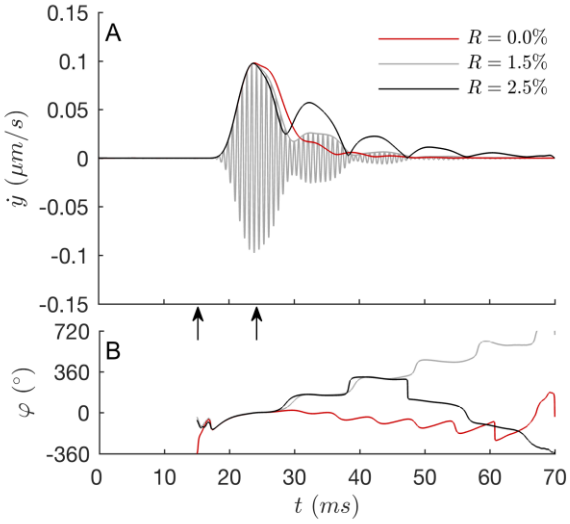

Figure 3: A: Simulated distortion product (f = 2 kHz; L_1 = 54 dB SPL; L_2 = 30 dB SPL; 1000 BM and TM segments) sampled at BM position x = 0 near the stapes for an active cochlea with roughness, R, of 1.5% (gray). Red and black lines depict the envelopes of distortion products computed without roughness and with R = 2.5%, respectively. Arrows indicate the onset and offset of the f_2 pulse. **B**: Phase signals for the distortion products shown in A.

3.2 Simulated distortion products

The model produces distortion products at the cubic difference frequency f_{DP} in response to input signals with two primary tones with frequencies f_1 and f_2 (f_2/f_1 = 1.2). Cancelation of the primary tones by averaging multiple simulation datasets with suitable primary-tone phases, allows visualization of the f_{DP} traveling wave. Consistent with the literature [3], the f_{DP} traveling wave emerges close to the f_2-tonotopic place and propagates to its own tonotopic place. Distortion products simulated in a smooth cochlea model, i.e. without irregularities in the mechanical parameters (R = 0), do not exhibit considerable contributions from the f_{DP}-tonotopic place (Figure 3A, red line), as evident by the absence of a second peak. In contrast, adding roughness to $k(x)$ and $F_{ca}(x,t)$ creates reflections and beat tones in the simulated signal (Figure 3A, gray and black lines).

Figure 4 depicts a DPOAE signal (gray line) recorded with f_2 = 2 kHz, L_2 = 35 dB SPL, and L_1 = 57 dB SPL. The red dashed lines show the envelopes of the extracted DPOAE components corresponding to, in order of their appearance, a

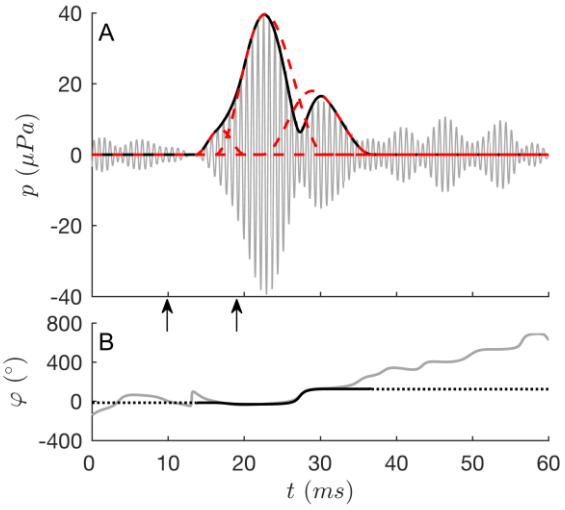

Figure 4: A: DPOAE signal (gray line) recorded with f_2 = 2 kHz (L_1 = 57 dB SPL, L_2 = 35 dB SPL). Red dashed lines: envelopes of computed DPOAE components associated with, in order of their appearance, a pre-component, the nonlinear-distortion component, and the coherent-reflection component. Black solid line: envelope of the vector sum of computed components. Arrows indicate onset and offset of f_2 pulse. **B**: Phase signals of the DPOAE signal (gray) and the vector sum of computed components (black).

pre-component, modelling the onset behavior or possible basal components of the DPOAE, the nonlinear-distortion component, and the coherent-reflection component. Besides the two main DPOAE components, both the simulated signal and the DPOAE recording exhibit additional components after the coherent-reflection component that become also apparent in the phase signals (cf. Figures 3B and 4B).

4 Discussion

The results provide further evidence for the coherent-reflection theory [3], which states that the f_{DP} traveling wave is partially reflected due to mechanical irregularities of the cochlear partition near its own tonotopic place. Incorporating roughness in the model generates additional components in the simulated signals, which cause wave interference with the fading nonlinear-distortion component, as evident in Figure 3A by the narrowing of the first peak and the occurrence of long-lasting beat tones. Both effects increase with increasing roughness and are also evident in the phase signals (Figure 3B) and in the measured DPOAEs (Figure 4). Simulated distortion products in the smooth cochlea, i.e. R = 0, indicate that minor phase changes during onset and offset of the DPOAE can be related to nonlinear amplification. In conclusion, comparison between simulated and measured signals shows that short stimulus pulses enable accurate estimation of the nonlinear-distortion component of DPOAEs in the time domain.

Author's Statement

Research funding: This work was supported by the German Research Council, Grant No. DFG Da 487/4-1 and Gu 194/12-1. Conflict of interest: Authors state no conflict of interest. Informed consent: Informed consent is not applicable. Ethical approval: The conducted research is not related to either human or animals use.

References

[1] Kemp DT. Evidence of mechanical nonlinearity and frequency selective wave amplification in the cochlea. Arch Otorhinolaryngol 1979; 224: 37–45.
[2] Robles L, Ruggero MA. Mechanics of the mammalian cochlea. Physiol Rev 2001; 81: 1305–1352.
[3] Shera CA, Guinan JJ Jr. Evoked otoacoustic emissions arise by two fundamentally different mechanisms: A taxonomy for mammalian OAEs. J Acoust Soc Am 1999; 105: 782–798.
[4] Dalhoff E, Turcanu D, Vetešník A, Gummer AW. Two-source interference as the major reason for auditory-threshold estimation error based on DPOAE input-output functions in normal-hearing subjects. Hear Res 2013; 296: 67–82.
[5] Zelle D, Gummer AW, Dalhoff E. Extraction of otoacoustic distortion-product sources using pulse basis functions. J Acoust Soc Am 2013; 134: EL64–69.
[6] Zelle D, Lorenz L, Thiericke JP, Gummer AW, Dalhoff E. Input-output functions of the nonlinear-distortion component of distortion-product otoacoustic emissions in normal and hearing-impaired human ears. J Acoust Soc Am 2017; 141: 3203–3219.
[7] Greenwood DD. A cochlear frequency-position function for several species – 29 years later. J Acoust Soc Am 1990; 87: 2592–2605.
[8] Gummer AW, Hemmert W, Zenner HP. Resonant tectorial membrane motion in the inner ear: Its crucial role in frequency tuning. Proc Natl Acad Sci 1996; 93: 8727–8732.
[9] Allen JB. Two-dimensional cochlear fluid model: New results. J Acoust Soc Am 1977; 61: 110–119.
[10] Mammano F, Nobili R. Biophysics of the cochlea: Linear approximation. J Acoust Soc Am 1993; 93: 3320–3332.
[11] Nobili R, Mammano F. Biophysics of the cochlea II: Stationary nonlinear phenomenology. J Acoust Soc Am 1996; 99: 2244–2255.
[12] Vetešník A, Gummer AW. Transmission of cochlear distortion products as slow waves: A comparison of experimental and model data. J Acoust Soc Am 2012; 131: 3914–3934.
[13] Whitehead ML, Stagner BB, Martin GK, Lonsbury-Martin BL. Visualization of the onset of distortion-product otoacoustic emissions, and measurement of their latency. J Acoust Soc Am 1996; 100: 1663–1679.